*34th EPS Conference on Plasma Phys. Warsaw, 2 - 6 July 2007 ECA Vol.**31F**, P-2.035 (2007)*

Fast Imaging of ELM Structure in DIII-D

J.H. Yu,[1] J.A. Boedo,[1] T.E. Evans,[2] E.M. Hollmann,[1] R.A. Moyer,[1]
D.L. Rudakov,[1] and P.B. Snyder[2]

[1]*University of California-San Diego, La Jolla, California 92093, USA*
[2]*General Atomics, San Diego, California 92186-5608, USA*

Edge localized modes (ELMs) are repetitive events observed during enhanced tokamak confinement regimes (H-mode) that result in the rapid loss of particles and heat from the plasma edge. Here we expand on previous measurements [1] and present fast-framed midplane images of ELMs in D_α and CIII light in the low-field plasma edge of the DIII-D tokamak. We find that ELMs are toroidally rotating helical filamentary structures that rapidly expand radially during the nonlinear phase. The inferred toroidal mode number n ranges from 10 to 35, and the mode number depends on plasma density [2]. The poloidal width of the filament ranges from 1 to 5 cm, and the location of the ELM-wall interaction due to cross-field transport of particles and heat is localized to within ±15 cm of the midplane.

ELMs are an important area of research because of potentially damaging effects to plasma facing components in future tokamaks and because of their role in wall recycling. Based on modeling and projections of existing observations, the number of ELMs (assuming a 10% loss of pedestal energy) that a divertor could tolerate in ITER may be as low as 500 [3]. However, results in high-density plasmas [4] show that the ELM energy may be sufficiently small for ITER to operate safely.

The experiments presented here have a lower single null configuration with plasma current I_p = 1.0–1.6 MA and toroidal field B_T = 2 T at the magnetic axis with major radius $R \sim 1.8$ m and minor radius $a \sim 0.6$ m. Injected neutral beam power is 5–9 MW. The fast camera is located approximately 2 m from the vessel due to space limitations and neutron shielding requirements. The camera has a semi-tangential view of the plasma emission viewed through a midplane window at toroidal angle $\phi = 90$ degrees, and an objective lens focuses the light onto the front face of an 8 x 10 mm coherent fiber-optic bundle. Over time, fusion neutrons degrade the transmission of the fiber bundle, particularly in the blue range of the visible spectrum, requiring that the bundle be periodically replaced. Light coming out the back of the fiber bundle is collimated and passed through an optical filter, and then focused onto a Vision Research Phantom v7.1 camera CMOS detector. The spatial resolution of the detector is 256 x 256 with 1 pixel imaging $(0.7\text{ cm})^2$ to $(0.4\text{ cm})^2$, depending on the location within the field of view. At this resolution, the camera is capable of storing 21,685 frames from one continuous movie with a maximum frame rate of 26,000 frames/s. Typical bandpass filters used here include central wavelengths of 465 nm for CIII emission and 656 nm for D_α emission.

Figure 1(a) shows images of an ELM in CIII light at four successive times marked in Fig. 1(b). The vertical field-of-view is approximately 90 cm and the main wall features that are visible include the rf antenna at $\phi = 0$ deg, a port at $\phi = 15$ deg, and the neutral beam injection (NBI) port at $\phi = 30$ deg. The tangential view of CIII emission provides direct visualization of the plasma edge and filaments in the scrape-off layer (SOL). However, low signal in CIII light limits the frame rate to ≤5,000 frames/s, and here the exposure time is 180 μs.

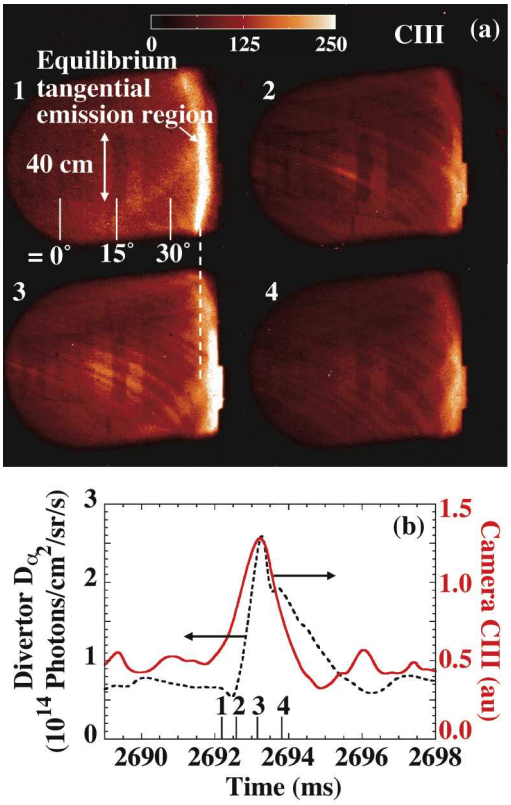

Fig. 1. (a) Images in CIII light of an ELM-driven plasma show multiple field-aligned filaments are ejected into the SOL. (b) The integrated camera intensity is compared to the inner divertor D_α signal, and the times of images 1–4 are labeled.

The first image in Fig. 1 shows that ELMs begin with an unstable filament that bulges radially outward near the low-field-side midplane. A single filament can be seen in the foreground of the image, immediately in front of the midplane viewing port at $\phi = 90$ deg. The pitch angle of this filament runs from the lower left to the upper right of the image (the slope of the foreground filament has the opposite sign as that of the filaments seen near the far wall in the other images, due to the viewing geometry). The observed filament pitch angle is consistent with the magnetic field pitch angle expected from edge EFIT values. During the nonlinear phase of the ELM (images 2 and 3), filaments convectively propagate radially outward into the SOL after ejection from the plasma edge. The radial displacement of the tangential emission region is seen by comparing the vertical dashed line in the first and third images (the first image has an effective gain 2x higher than the other images). The integrated emission increases by a factor of 2 to 4 as particles are ejected outward into the ~6 to 10 eV temperature region of high CIII excitation. Once in the SOL, particles and heat undergo rapid parallel transport to the divertor. However, a significant fraction of the ejected particles move sufficiently fast across field lines, and images in D_α light (not presented here) show filaments interacting with the outer-midplane wall. Interestingly, when an ELM hits the carbon wall, the relative increase in D_α emission is much larger than the increase in CIII emission (both compared to inter-ELM images), possibly suggesting that ELM-wall interactions release deposited deuterium from the wall more readily than carbon. Similar to previous measurements [5], fast images show that individual filaments are ejected at different

times during a single ELM, that is, an ELM appears as a packet of filaments ejected from the plasma edge in succession.

Figure 1(b) shows the ELM time signal obtained by integrating the intensity from each camera frame, and the D_α signal (dashed) measured at the inner divertor is shown for reference. Comparing these signals during multiple events shows that ELMs in high collisionality plasmas originate at the outer midplane in agreement with previous measurements of radiated power and supporting the theoretical picture of ELMs driven by the peeling-ballooning instability. However, in low collisionality plasmas the peak midplane and divertor ELM signals appear simultaneously, possibly indicating a global mode structure for large ELMs that appear in low-density plasmas.

The mode structure of filaments at the onset of ELMs is measured from the toroidal separation $\Delta\phi$ of adjacent filaments, and Fig. 2 shows the toroidal mode number $n \equiv 2\pi/\Delta\phi$ versus pedestal density $n_{e,ped}$. A general trend in the data shows that ELMs are smaller and have a higher toroidal mode number at high density, while low-density plasmas have a lower mode number [2]. These results are consistent with ELITE [6] code calculations showing that the most unstable n increases as the edge current density decreases, which is expected at high density due to collisional suppression of the bootstrap current.

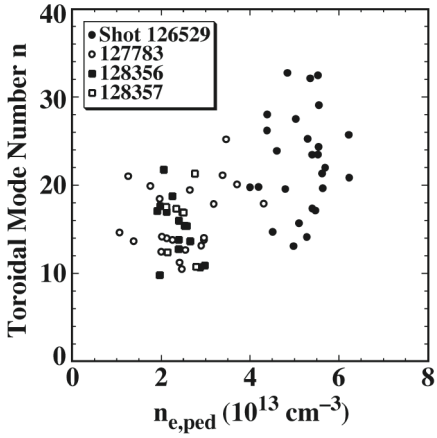

Fig. 2. Measured ELM toroidal mode number versus pedestal density.

Images of ELM-wall interaction in D_α light with exposure time of 31 μs are used to measure the distribution of locations where ELM filaments hit the midplane wall. The particle and heat flux to the divertor targets due to parallel transport in the SOL are not considered here, because the divertor is outside the fast camera field-of-view. When an ELM filament interacts with the wall, a bright stripe of emission is caused by release of neutrals from the wall tiles. A 1D vertical profile of the light intensity at a wall location of ϕ=12 deg during an ELM-wall interaction is obtained by subtracting background (inter-ELM) light, and a Gaussian fit is made to the 1D perturbation profile signal during the peak ELM intensity. The poloidal full-width-half-maximum w of the filament and vertical location Z_{ELM} of the ELM-wall interaction are then recorded during a high density discharge, with $\langle n_e \rangle / n_{GW} = 0.7$ where n_{GW} is the Greenwald density. Figure 3(a) shows that the distribution of

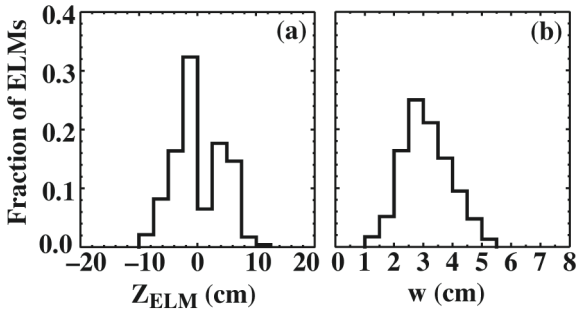

Figure 3. Distributions of (a) location Z_{ELM} where ELM filaments hit the outer wall, and (b) poloidal filament width w.

ELM-wall interactions is localized to within ±15 cm of the midplane, suggesting that sensitive diagnostics could be placed above or below the midplane to avoid possible damage in future devices. The poloidal (or vertical) filament width ranges from 1 to 5 cm, with a mean poloidal width of 3 cm as shown in Fig. 3(b). This width roughly agrees with previous probe measurements [5] of individual filaments transiting the probe location in a time of 20 to 40 μs at a radial velocity of 500 to 1000 m/s.

Fast imaging of ELMs in the low-field-side midplane of DIII-D demonstrates that ELMs begin with toroidally and poloidally localized unstable filaments bulging radially outward, and that multiple filaments are ejected into the SOL in rapid succession within a few hundred μs. Due to cross-field transport, a significant fraction of ELMs interact with the midplane wall and release neutrals, and the interactions are localized to within ±15 cm of the midplane. The filament widths range from 1 to 5 cm, which agrees with previous estimates based on probe measurements. Fast imaging data presented here are consistent with the peeling-ballooning theory for ELMs, which postulates that ELMs are a limit cycle driven by a combination of current and pressure-gradient MHD instabilities [6,7]. In addition, recent nonlinear calculations of ELMs using the BOUT code show similar phenomena compared with the camera observations, including the initial explosive growth of a single filament and then possible secondary instabilities causing radial break up into several filaments [8].

This work was supported by the U.S. Department of Energy under DE-FG02-04ER54758 and DE-FC02-04ER54698. J.H. Yu thanks Dr. Antar for the initial conceptual design of the camera system.

References

[1] G. Antar, *et al.,* these proceedings.
[2] T.H. Osborne, *et al.*, Proc. 29th EPS Conf. on Plasma Phys. and Control. Fusion, Montreux, 2002, ECA Vol. **26B**, P-1.062 (2002).
[3] G. Federici, *et al.,* J. Nucl. Mater. **313-316**, 11 (2003).
[4] A.W. Leonard, *et al.,* J. Nucl. Mater. **290-293**, 1097 (2001).
[5] J.A. Boedo, *et al.,* Phys. Plasmas **12**, 072516 (2005).
[6] P.B. Snyder, *et al.,* Phys. Plasmas **9**, 2037 (2002).
[7] H.R. Wilson, *et al.,* Plasma Phys. Control. Fusion **48**, A71 (2006).
[8] P.B. Snyder, *et al.,* Phys. Plasmas **12**, 056115 (2005).